



# Interaction of Nitrate Assimilation and Photorespiration at Elevated CO<sub>2</sub>

Konrad Krämer, Judith Brock and Arnd G. Heyer\*

Department of Plant Biotechnology, Institute of Biomaterials and Biomolecular Systems, University of Stuttgart, Stuttgart, Germany

## OPEN ACCESS

### Edited by:

Guillaume Pilot,  
Virginia Tech, United States

### Reviewed by:

Toshihiro Obata,  
University of Nebraska-Lincoln,  
United States  
Pavel Kerchev,  
Mendel University in Brno, Czechia  
Michael Hodges,  
UMR9213 Institut des Sciences des  
Plantes de Paris Saclay (IPS2),  
France

### \*Correspondence:

Arnd G. Heyer  
arnd.heyer@bio.uni-stuttgart.de

### Specialty section:

This article was submitted to  
Plant Physiology,  
a section of the journal  
Frontiers in Plant Science

Received: 16 March 2022

Accepted: 07 June 2022

Published: 01 July 2022

### Citation:

Krämer K, Brock J and  
Heyer AG (2022) Interaction of Nitrate  
Assimilation and Photorespiration at  
Elevated CO<sub>2</sub>.  
Front. Plant Sci. 13:897924.  
doi: 10.3389/fpls.2022.897924

It has been shown repeatedly that exposure to elevated atmospheric CO<sub>2</sub> causes an increased C/N ratio of plant biomass that could result from either increased carbon or – in relation to C acquisition - reduced nitrogen assimilation. Possible reasons for diminished nitrogen assimilation are controversial, but an impact of reduced photorespiration at elevated CO<sub>2</sub> has frequently been implied. Using a mutant defective in peroxisomal hydroxy-pyruvate reductase (*hpr1-1*) that is hampered in photorespiratory turnover, we show that indeed, photorespiration stimulates the glutamine-synthetase 2 (GS) / glutamine-oxoglutarate-aminotransferase (GOGAT) cycle, which channels ammonia into amino acid synthesis. However, mathematical flux simulations demonstrated that nitrate assimilation was not reduced at elevated CO<sub>2</sub>, pointing to a dilution of nitrogen containing compounds by assimilated carbon at elevated CO<sub>2</sub>. The massive growth reduction in the *hpr1-1* mutant does not appear to result from nitrogen starvation. Model simulations yield evidence for a loss of cellular energy that is consumed in supporting high flux through the GS/GOGAT cycle that results from inefficient removal of photorespiratory intermediates. This causes a futile cycling of glycolate and hydroxy-pyruvate. In addition to that, accumulation of serine and glycine as well as carboxylates in the mutant creates a metabolic imbalance that could contribute to growth reduction.

**Keywords:** photorespiration, nitrate assimilation, elevated CO<sub>2</sub>, hydroxypyruvate reductase, *Arabidopsis*

## INTRODUCTION

In the course of climate change a substantial increase of the atmospheric CO<sub>2</sub> concentration is expected for the 21st century (IPCC, 2014; Szulejko et al., 2017). Because CO<sub>2</sub> is the substrate for plant photosynthesis, alteration in the CO<sub>2</sub> level have a direct impact on plant metabolism. The enzyme ribulose-1,5-bisphosphat-carboxylase/oxygenase (RUBISCO) catalyses CO<sub>2</sub> fixation, but can also use O<sub>2</sub> as substrate, resulting in the production of 2-phosphoglycolate, which is then further processed in the so-called photorespiration (PR) pathway (Shih et al., 2015). Because carboxylation is preferred over oxygenation (Sharkey, 1988), elevated CO<sub>2</sub> concentrations (eCO<sub>2</sub>) will distinctly reduce the probability of oxygenation of RUBISCO (Sharkey, 1988), and thus flux through the PR pathway will decline. Considering that a large proportion of the amino acids glycine (Gly) and serine (Ser) are produced during PR, this will affect plant primary metabolism.

In the course of PR two molecules of 2-phosphoglycolate (2-PG) are converted to one molecule of 3-phosphoglycerate, which is fed back into the Calvin-Benson-Cycle

(Huma et al., 2018). More precisely, 2-PG is converted to glycolate which is subsequently oxidized to glyoxylate, producing H<sub>2</sub>O<sub>2</sub> as a byproduct in peroxisomes. Next, glyoxylate is transaminated to Gly. The N source is either Ser or glutamate (Glu), resulting in the production of hydroxypyruvate and  $\alpha$ -Ketoglutarate ( $\alpha$ -KG), respectively (Nunes-Nesi et al., 2010). Hydroxypyruvate is reduced by the hydroxypyruvate-reductase (HPR) forming glycerate which can be phosphorylated to 3-phosphoglycerate (Timm et al., 2008). Gly is transported to mitochondria, where it is used by the glycine-decarboxylase (GDC), converting Gly, NAD<sup>+</sup> and tetrahydrofolic acid to NADH, CO<sub>2</sub>, NH<sub>4</sub><sup>+</sup> and N<sup>5</sup>, N<sup>10</sup>-methylene-tetrahydrofolic acid. The CO<sub>2</sub> evolution in this step is eponymous for the PR (Rebeille et al., 1994). Together with N<sup>5</sup>, N<sup>10</sup>-methylene-tetrahydrofolic acid a second molecule of Gly is converted to Ser by the enzyme serine-hydroxymethyl transferase (SHMT). Ser is transported to the peroxisomes, where it serves as N donor for Gly production from glyoxylate, yielding hydroxypyruvate (Nunes-Nesi et al., 2010). Besides energy consumption, the oxygenation of RUBISCO and the subsequent PR create toxic intermediates such as 2-PG, glycolate and glyoxylate, which must be removed quickly (Anderson, 1971; Dellerio et al., 2016). Even though the entire pathway, starting from oxygenation of ribulose-bisphosphate, appears wasteful, there is strong evidence that PR plays a role in the response to abiotic stress (Voss et al., 2013), for photoprotection (Guan et al., 2004) and nitrogen (N) assimilation (Cousins and Bloom, 2004; Bloom, 2015; Kraemer et al., 2021a).

Nitrogen assimilation mainly starts from nitrate that is reduced to nitrite and subsequently to ammonium by nitrate reductase (NR) and nitrite reductase, respectively (Xu et al., 2012). Ammonium is used to produce glutamine, the acid amide of Glu, catalyzed by glutamine synthetase (GS). The net synthesis of amino acids is then accomplished by the enzyme glutamine-oxoglutarate aminotransferase (GOGAT), which produces two molecules of Glu. Thus, the two enzymes GS and GOGAT create a cycle of Glu synthesis and amination that consumes ammonium,  $\alpha$ -KG, ATP and reducing equivalents and yields Glu (Selinski and Scheibe, 2019).

Bloom (2015) proposed that increased PR flux causes higher malate levels in the cytosol. These could maintain turnover in the GS/GOGAT cycle and, concomitantly, produce NADH as substrate for NR. However, Andrews et al. (2019) showed that eCO<sub>2</sub> affects N assimilation independently of the form of N administered, and that no inhibition of nitrate assimilation occurs. Thus, the mechanism by which eCO<sub>2</sub> interferes with N assimilation remains unclear. Using a mathematical model that was parameterized by literature data, Zhao et al. (2021) demonstrated evidence that  $\alpha$ -KG becomes limiting for N assimilation under eCO<sub>2</sub>, and we have obtained similar results investigating photosynthetic acclimation to eCO<sub>2</sub> (Kraemer et al., 2021a). Because  $\alpha$ -KG is central in the GS/GOGAT cycle, this again puts the PR pathway in focus. In this study we investigate the role of PR flux for N assimilation. We compare *Arabidopsis thaliana* plants grown at either ambient or eCO<sub>2</sub>. To create different

PR fluxes, we used the *hpr1-1* mutant which lacks peroxisomal HPR (Timm et al., 2008) This results in elevated levels of Gly and Ser (Timm et al., 2021), stunted growth at ambient CO<sub>2</sub> and a chlorotic phenotype (Li et al., 2019). The mutant shows elevated levels of  $\alpha$ -KG and free amino-acids (Timm et al., 2021). We propose that growth reduction in the mutant is at least partly due to a disturbed energy household resulting from insufficient linear flux through PR.

## MATERIALS AND METHODS

### Plant Growth and Photosynthesis Measurement

*A. thaliana* wildtype Col-0 and the mutant *hpr1-1* (SALK067724) were grown in hydroponic culture for 50 days in a growth chamber with 8 h/16 h light/dark regime (100  $\mu$ mol m<sup>-2</sup> s<sup>-1</sup>; 22°C/16°C). For the first 17 days plants were grown at ambient CO<sub>2</sub> (450  $\pm$  20 ppm). Afterwards half of the plants were transferred to eCO<sub>2</sub> (1,000  $\pm$  20 ppm). The hydroponic medium was as described in Brauner et al. (2014) with the difference that no ammonium was supplied and the nitrate concentration reduced to 2.175 mM. This assured sufficient, but not excess supply of N as identified in experiments with different levels of nitrate supply. For measurements of metabolites and enzyme activities, full rosettes of 50 day old plants were harvested every 2 h over a full diurnal cycle at fivefold replication under ambient as well as eCO<sub>2</sub>, resulting in a total of 120 samples. Photosynthesis measurements were conducted 1 week before harvesting as described by Küstner et al. (2019). Briefly, an infrared gas analysis system (Uras 3G; Hartmann and Braun AG, Frankfurt am Main, Germany) equipped with five custom made whole-rosette cuvettes and a sixth channel for measurement of CO<sub>2</sub> in surrounding atmosphere was operated at a flow rate of 40 l/h, and each of the channels was measured sequentially for 6 min over a full diurnal cycle at a rate of 0.1 Hz. From the measured time points, splines were generated to yield a complete course of photosynthetic activity. All measurements were conducted at growth light and the respective CO<sub>2</sub> concentration. Using the result of the photosynthesis measurements the photorespiratory activity was calculated according to the method developed by Sharkey (1988). For  $\Gamma^*$  the values identified by Kraemer et al. (2021a) were used. As a first step, the ratio between oxygenation and carboxylation-  $\Phi$ -was calculated according to equation (1).

$$\Phi = \left( 2^* \Gamma^* \right) / \text{Temperature} \quad (1)$$

Using this ratio the rate of oxygenation was calculated according to equation (2).

$$v_o = (\text{PS} - \text{Respiration}) / (1 / \Phi - 0.5) \quad (2)$$

The photorespiratory activity used in the model was calculated as the oxygenation rate divided by 2.

## Metabolite Measurements

Gly, Ser,  $\alpha$ -KG, glucose, fructose and sucrose were measured by quantitative GC–MS/MS. Samples were extracted using 750  $\mu$ l methanol with 25 nmol ribitol as internal standard. After 15 min at 70°C followed by shaking for 10 min at RT samples were centrifuged (5 min 17,000 g). The supernatant was transferred to a new vessel, and 400  $\mu$ l of H<sub>2</sub>O were added. After incubation for 10 min at 95°C samples were agitated for 10 min at RT. Following centrifugation (5 min, 17,000 g) the supernatants were pooled. Subsequently, 300  $\mu$ l H<sub>2</sub>O and 200  $\mu$ l chloroform were added. After centrifugation (2 min, 17,000 g) the two phases were separated and the polar phase was dried in a speedvac and used for analysis. Dried samples were derivatized using 20  $\mu$ l of methoxamine dissolved in pyridine (40 mg/ml) by incubation for 90 min at 30°C. Next, 80  $\mu$ l N-methyl-N-(trimethylsilyl)trifluoroacetamide (MSTFA) were added and the solution was incubated for 30 min at 50°C. Metabolites were measured by gas-chromatography coupled to mass-spectrometry (GC–MS/MS). For injection, 1  $\mu$ l of the derivatized sample was used. The GC–MS/MS device was a GCMS-TQ8040 (Shimadzu, Kyoto, Japan) using helium as carrier gas at a flow of 1.12 ml/min. The stationary phase was a 30 m Optima 5MS-0.25  $\mu$ m fused silica capillary column. Injection temperature was 230°C. The transfer line and ion source were set to 250°C and 200°C, respectively. The initial temperature of the column oven was 80°C and this was increased by 15°C/min until the final temperature of 330°C was reached and held for 6 min. After a solvent delay of 4.6 min, spectra of the MS device were recorded in the multiple reaction mode (MRM) with specific target-ions for each metabolite. External standards were used for quantification.

Starch, hexose-phosphates and the total amino-acid pool were determined photometrically and carbonic acids (fumaric acid, malic acid and citric acid) by HPLC as described by Küstner et al. (2019). Ammonium was quantified according to Vega-Mas et al. (2015). Glu and Gln were measured according to Graham and Aprison (1966) and Pérez-de la Mora et al. (1989).

## Enzymatic Activities

Activity of nitrate reductase was measured as described by Scholl et al. (1974). Activity of hydroxy-pyruvate-reductase was determined according to Bauwe (2017). GS activity was measured according to Berteli et al. (1995) and Silveira et al. (2003). Briefly, protein was extracted into a 100 mM Tris–HCl (pH 7.6) buffer containing 2.5 mM dithiothreitol and 10 mM MgCl<sub>2</sub>. The assay buffer contained 125 mM Tris–HCl (pH 7.6), 5 mM ATP, 80 mM MgSO<sub>4</sub>, 125 mM hydroxylamine–NaOH (pH 7) and 100 mM glutamate (pH 7.2). To an assay buffer volume of 80  $\mu$ l, 120  $\mu$ l of protein extract were added and incubated for different time-points (0, 20, 25 and 30 min). To determine the background, an assay buffer was used without hydroxylamine–NaOH (pH 7). The reaction was stopped using 60  $\mu$ l of a solution consisting of 1.5 ml 10% w/v FeCl<sub>3</sub>·6 H<sub>2</sub>O in 0.2 N HCl, 1.5 ml 24% w/v trichloroacetic acid and 1.5 ml 20% v/v HCl. Afterwards, the absorption was determined at 540 nm. For calibration curves L-glutamic acid  $\gamma$ -monohydroxamate was used.

All enzyme activities were determined at the beginning, middle and end of the light phase as well as in the middle of the night. Values for the remaining time-points were calculated by spline interpolation. For the calculation of reaction velocity, substrate concentration was calculated from the measured metabolite contents, assuming that 1 g of plant biomass had a volume of 0.77 ml.

## Data Analysis and Statistics

Data evaluation, normalization, visualization and statistics were performed in Microsoft Excel (RRID:SCR\_016137) and the R software (R Project for Statistical Computing, RRID:SCR\_001905). The experimental design was a randomized complete block design with CO<sub>2</sub> level as block and genotype as treatment. If not otherwise stated, two-way ANOVA for genotype and CO<sub>2</sub> treatment effects were used for statistical analysis. Parameter optimization was performed in a way that *in silico* time courses best matched the measured time courses. For optimization and simulations the R-package *paropt* was used (Kraemer et al., 2021b).

## RESULTS

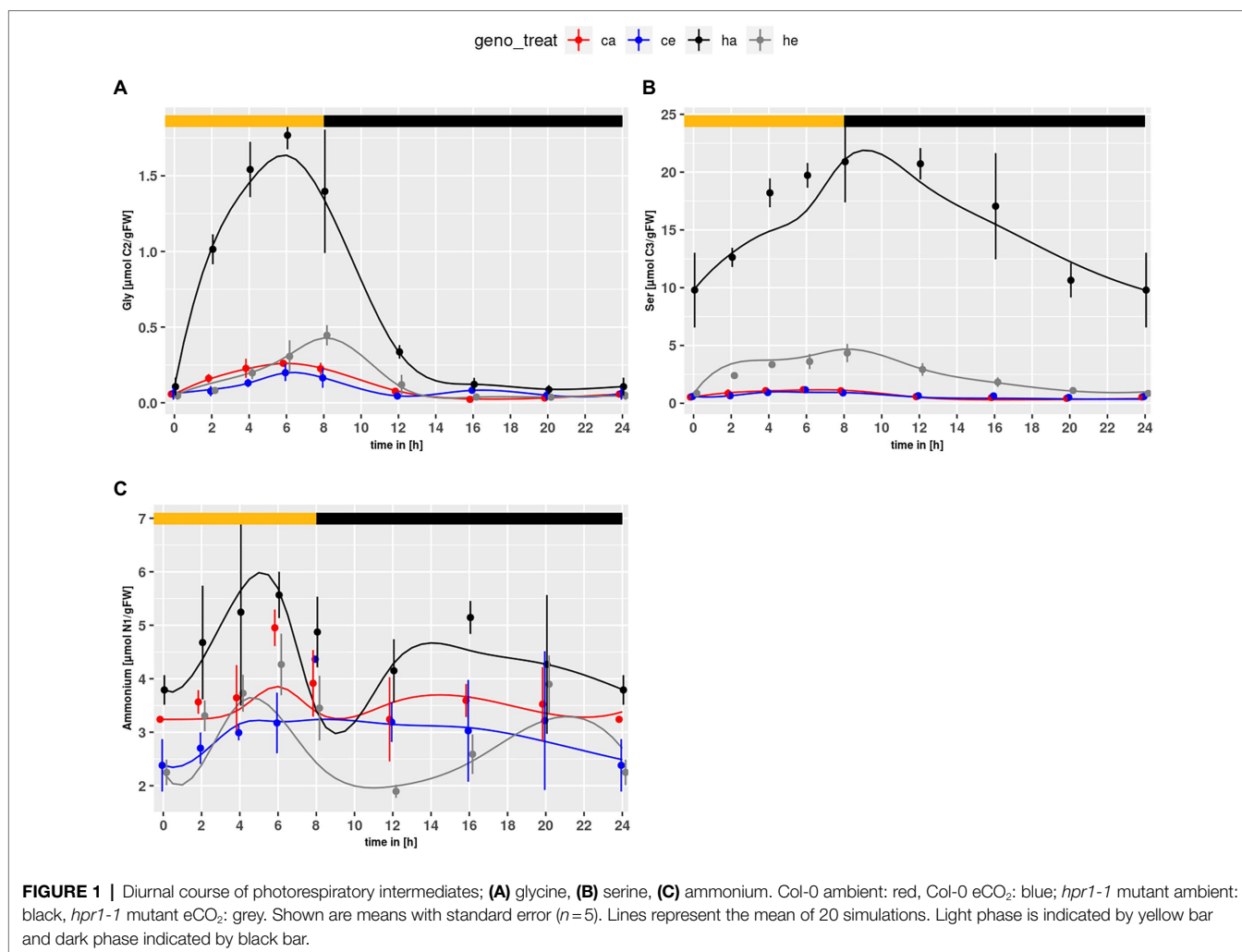
### Diurnal Dynamics of Metabolites

Net photosynthetic rates (*PS*) increased by about 50% in the wildtype, when CO<sub>2</sub> concentration was raised to 1,000 ppm. The wildtype had significantly higher *PS* than the mutant ( $p < 2e-16$ ) under both conditions (Col-0 at ambient CO<sub>2</sub> = 85.4  $\pm$  12.8  $\mu$ mol/g \* h, Col-0 at eCO<sub>2</sub> = 128.1  $\pm$  44.9  $\mu$ mol/g \* h, *hpr1-1* at ambient CO<sub>2</sub> = 76.8  $\pm$  19.9  $\mu$ mol/g \* h, *hpr1-1* at eCO<sub>2</sub> = 98.6  $\pm$  35.8  $\mu$ mol/g \* h). An increase in net photosynthesis by about 50% at eCO<sub>2</sub> in the wildtype is in accordance with previous observations (Jauregui et al., 2016). However, a stronger reduction of photosynthesis in *hpr1-1* was reported for higher light intensities by Timm et al. (2008).

Despite the lower *PS* rate and no obvious deviations in hexose-phosphate levels (**Supplementary Image 1**), the combined pool of malate and fumarate (MF) was larger in the *hpr1-1* mutant than in wildtype ( $p = 4.1e-10$ ). Citrate (Cit) was elevated in *hpr1-1* only at ambient CO<sub>2</sub> (**Supplementary Image 1**;  $p = 2.47e-7$ ) and showed a different response to rising CO<sub>2</sub> levels: while it increased in the wildtype ( $p = 7.1e-4$ , *t*-test for wildtype), it declined in the mutant ( $p = 5.08e-6$ , *t*-test for *hpr1-1*).

The PR intermediates Gly and Ser accumulated in the mutant under both conditions (**Figures 1A,B**). As expected, the contents were higher at ambient CO<sub>2</sub>. For NH<sub>4</sub><sup>+</sup>, which is also produced during PR, significant genotype and treatment effects were observed with higher levels in *hpr1-1* and a general decrease under eCO<sub>2</sub> ( $p = 5.67e-5$  and  $p = 4.38e-6$ , respectively).

Similar to the NH<sub>4</sub><sup>+</sup> content, Glu levels (**Figure 2A**) were elevated in the mutant as compared to wildtype ( $p = 7.71e-4$ ) and significantly increased in mutant plants at ambient CO<sub>2</sub> as compared to eCO<sub>2</sub> ( $p = 2.03e-10$ ). This effect could not be observed for Col-0. Neither genotype nor treatment effects were observed for Gln (**Figure 2B**). However, when considering



the mutant alone, an elevated level at ambient CO<sub>2</sub> became obvious ( $p=0.0163$ ). The  $\alpha$ -KG content (**Figure 2C**) was strongly increased for *hpr1-1* at ambient CO<sub>2</sub>. Considering that Glu is converted to  $\alpha$ -KG when used as substrate for transamination of glyoxylate in the peroxisome, elevated  $\alpha$ -KG may point to an increased Glu turnover for transamination of glyoxylate.

Furthermore, the amino acid (AA) pool (**Figure 2D**) was elevated in the mutant compared to wildtype ( $p < 2.0e-16$ ). Considering only mutant data, an increase at eCO<sub>2</sub> was significant ( $p < 2.0e-16$ ). Thus, no indications for N-starvation in the mutant were found.

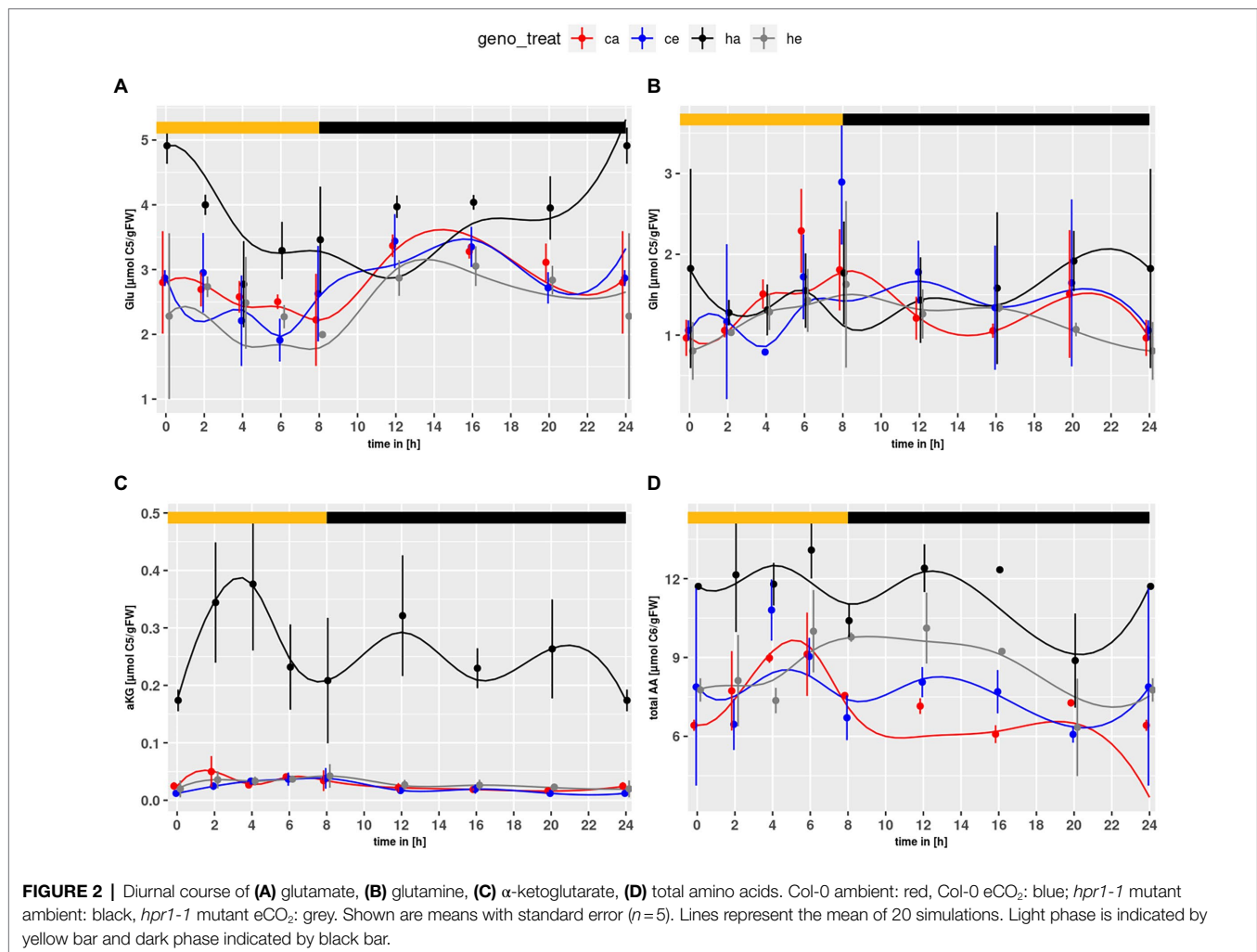
## Diurnal Dynamics of Parameters for Enzyme Activity

Maximum activities were determined for three enzymes central to *de novo* N assimilation, amino acid metabolism and PR. For NR, the Col-0 wildtype showed the highest activity at eCO<sub>2</sub> (**Supplementary Image 2A**). This constituted a significant genotype effect ( $p=0.0346$ ) that was unexpected considering reports of decreased N assimilation at eCO<sub>2</sub> (Bloom et al., 2014). In addition, a time effect with highest activity at midday

was observed independent of the condition ( $p=0.0017$ ). GS activity (**Supplementary Image 2B**) was clearly affected by the CO<sub>2</sub> level with higher activity at ambient CO<sub>2</sub> than at eCO<sub>2</sub> ( $p=4.14e-13$ ). Notably, *hpr1-1* had even higher GS activity than Col-0 when grown at ambient CO<sub>2</sub> ( $p=0.0021$ ), indicating a higher potential for turnover in the GS/GOGAT cycle. Not surprisingly, a genotype effect was found for HPR activity (**Supplementary Image 2C**;  $p < 2e-16$ ). In addition, a treatment effect was detected, which was dependent on the *hpr1-1* data ( $p=0.0461$ ).

## Model Construction

With the aim of mathematically simulating C/N interactions at eCO<sub>2</sub>, a dynamic model based on ordinary differential equations (ODE) was constructed that covered carbon as well as nitrogen acquisition. The model structure is depicted in **Figure 3**. Based on measurements of photosynthesis and respiration as well as metabolite content at 8 time points over a diurnal cycle, kinetic parameters were identified that allowed simulation of metabolite dynamics with only the metabolite levels at the beginning of the light period ( $t=0$ ) given. The identified parameters (see **Supplementary Table 1**) describe

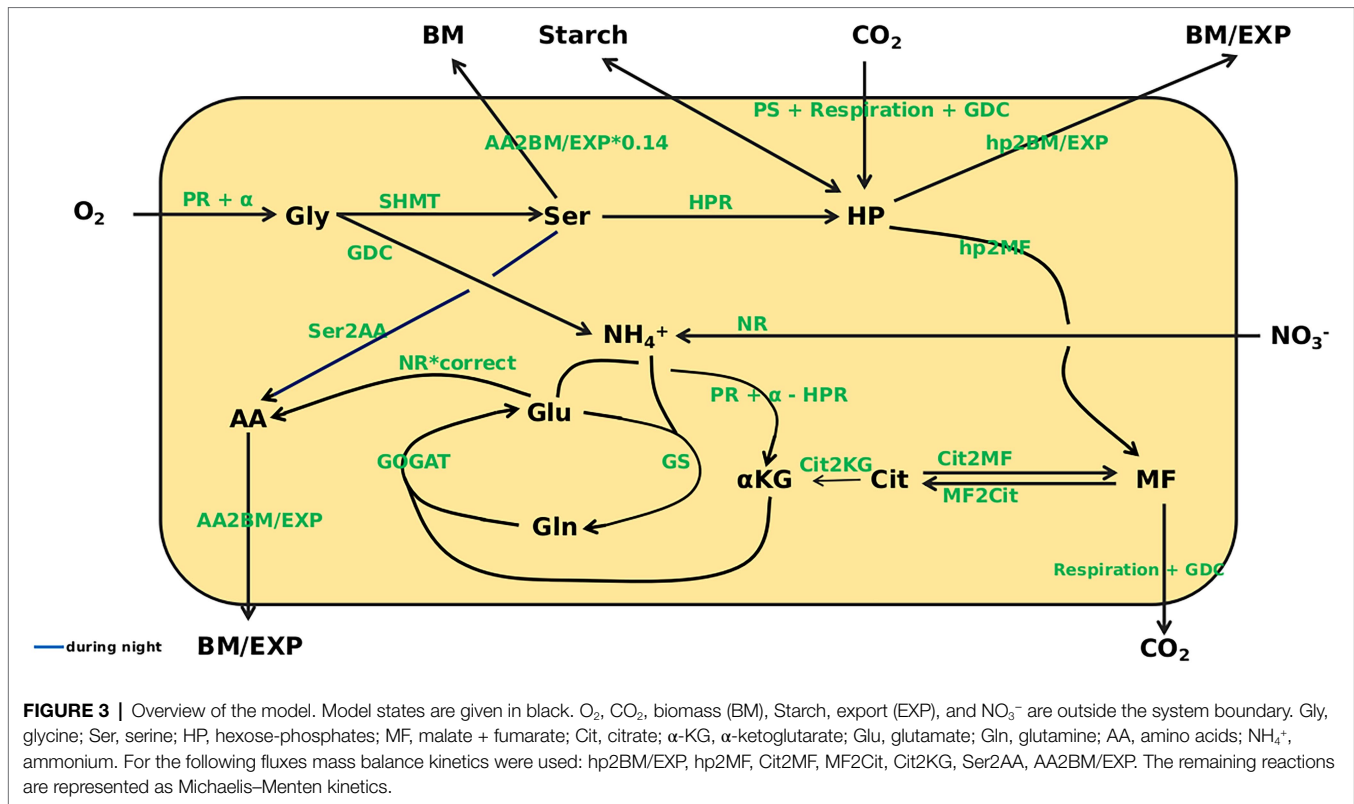


turnover rates for C- and N-compounds. Besides concentrations of O<sub>2</sub> and CO<sub>2</sub>, the plant biomass (BM), starch level, amount of assimilates exported from the leaves (EXP) and nitrate level are regarded as beyond the system boundaries, which means that, e.g., the rate of starch synthesis is included in simulations, but not the actual amount that has accumulated at a certain time point. In contrast, levels of Gly, Ser, HP, MF, Cit, α-KG, Glu, Gln, AA and NH<sub>4</sub><sup>+</sup> are included in the simulations. For the carbon fluxes to biomass and sink organs (*hp2BM/EXP*; note: all fluxes in italics), to or among carboxylic acids (*hp2MF*, *Cit2MF*, *MF2Cit*, *Cit2KG*), as well as the C/N fluxes from serine to amino acids (*Ser2AA*) and amino acids to biomass and export (*AA2BM/EXP*), mass balance kinetics were applied. The remaining reactions are represented as Michaelis–Menten kinetics. Kinetic equations for enzyme reactions are given in file **Supplementary Data Sheet 1**. The full ODE system is given in file **Supplementary Data Sheet 2**.

Initial steps of the PR pathway are represented by a reaction yielding Gly, which means that all reactions from oxygenation of ribulose-bisphosphate to glyoxylate formation were not resolved, because absolute quantification of the respective intermediates is not reliable. Input into the pathway

was calculated on the basis of PS according to Sharkey (1988). Gly is converted to Ser, which was considered precursor for the HPR reaction that feeds back into the pool of sugar-phosphates. Alternatively, Ser can flow into the pool of the other AA, representing the reaction of Ser-pyruvate aminotransferase.

All short-lived intermediates of the Calvin-Benson-Cycle, triose-phosphates and hexose-phosphates were represented by the HP pool, which is quantitatively dominated by glucose-6-phosphate and fructose-6-phosphate. The latter were quantified enzymatically (see Material and Methods). Photosynthesis, measured as CO<sub>2</sub> uptake per time, constituted the carbon input into this pool. Measured values were corrected for mitochondrial respiration and PR input. Mitochondrial respiration was measured during the dark phase and set constant over the entire diurnal cycle as earlier suggested by Küstner et al. (2019) and Krämer et al. (2021a). The HP pool was set as the precursor for cell wall synthesis and the supply of carbon to sinks. It should be mentioned that the transport metabolite, sucrose, attains much higher levels than measured for HP, which is substrate for cell wall biosynthesis. While this would affect the ratio of BM formation and transport rates, when kinetic parameters



are constrained, this was not the case in the current model, which left wide ranges for the BM/EXP parameter, because assimilate export was not in focus. In the model, assimilate export and biomass formation were represented by the combined flux  $hp2BM/EXP$ . In addition, HP is in exchange with starch that serves as carbon source during the night. Starch production during the day and degradation at night was assumed to be linear as outlined by Stitt and Zeeman (2012). As demonstrated by Gauthier et al. (2010) and Tcherkez et al. (2009), Cit is not, or only to a very low extent, produced during the day, but accumulates during the night and is used for α-KG production during the next day (Cheung et al., 2014). Therefore, the substrate for accumulation of MF during the light phase was considered to be HP, thus referring to anaplerotic reactions. However, the possibility of a flux from Cit to MF was not excluded. MF is used for mitochondrial respiration.

During the reaction from Gly to Ser NH<sub>4</sub><sup>+</sup> is produced and, together with Glu, can be used by GS to produce Gln (Supplementary Image 2). Gln can transaminate α-KG, catalyzed by GOGAT, to produce two molecules of Glu. Two reactions can yield α-KG that is required for AA production. The first reaction is from Cit (Cheung et al., 2014) representing the TCA cycle and cytosolic isocitrate dehydrogenase activity (Hodges, 2002). The second is from Glu and includes the reaction of Glu-glyoxylate-aminotransferase, which is part of PR, as well as mitochondrial Glu dehydrogenase and transamination reactions involving Glu. For Gly production, a source of N is required. This can derive from Ser, which, in the model, is included in the combined HPR flux. Alternatively,

Glu can serve as N donor for Gly production. The PR flux into the system, the HPR flux, and the reaction from Glu to α-KG are all N<sub>1</sub>-fluxes. Thus, the three fluxes can be balanced, and Glu to α-KG can be expressed as PR minus HPR.

Another source of NH<sub>4</sub><sup>+</sup> is the reduction of nitrate by NR (Supplementary Image 2). Modeling this *de novo* N fixation is complicated by the fact that a large proportion of nitrate is stored in the vacuole and not accessible by NR. To account for this compartmentation, the content was adjusted based on the cellular proportion of cytosol, which is about 5% of total cell volume in mature leaves (Koffler et al., 2013). NR is the only flux providing *de novo* assimilated N. Thus, the step towards AA production was linked to NR. According to Gauthier et al. (2010) about 50% of Ser consist of newly assimilated N. Accordingly, we modeled the flux from Glu to AA as NR multiplied by the correction factor, *correct*, which was set in the interval [0.5, 1]. Because the PR intermediates Gly and Ser are the only other sinks for *de novo* assimilated N in our model, *correct* likewise determines the deposition of new N in these compounds.

Because PR flux, as defined by Sharkey (1988), is directly coupled to photosynthetic activity, the pathway would not operate in the dark, which would, in our model, exclude turnover of Gly and Ser after light-off. However, especially in the case of *hpr1-1* at ambient CO<sub>2</sub>, Ser turnover was substantially extended into the night. This was accounted for by adding the summand α to the formula for PR, which allows operation of pathway reactions described by Walton and Butt (1981) independent of photosynthetic activity.

The step from Gly to Ser is catalyzed by the two enzymes *GDC* and *SHMT*. For both reactions Michaelis–Menten kinetics were employed. However, turnover of *SHMT* cannot exceed that of *GDC*, and thus *SHMT* was limited to the *GDC* value. In contrast, it is known from the literature that the *GDC* flux may well be substantially higher than the flux of *SHMT* (Rebeille et al., 1994).

Because the model structure presented in **Figure 3** does not allow the amino acids Gly and Ser to contribute to biomass via the *AA2BM/EXP* route, a separate pathway was established for these compounds. Based on proteome information for *Arabidopsis* (Berardini et al., 2015) a proportion of about 10% of the amino acids in protein should be Ser. However, Rubisco, which makes up about one third of total protein (Atkinson et al., 2017), has 14% Ser, and thus, the flux from Ser to BM was set to 14% of the flux from AA to BM/EXP.

## Preliminary Parameter Identification

According to the above described model structure several rounds of parameter optimization were conducted that yielded results for most states that were covered by the measured standard deviation with an averaged error between 0.05 and 0.1% per state and time point. However, Glu levels were consistently underestimated, particularly during the night as shown in **Figure 4A**. Choi et al. (1999) reported that the GS enzyme of *Canavalia lineata* is activated by a reduction at two cysteine residues, which are conserved among all known plastidial GS sequences. The authors demonstrated that reductants like dithiothreitol increase the activity of the plastidial isoform. Considering that dithiothreitol was added during protein extraction (see “Materials and Methods”), it is very likely that GS activity was overestimated, especially during the night. It is known that, following light-off, the redox milieu of the chloroplasts changes rapidly (Dietz and Hell, 2015). However, the extent of change in GS activity is unknown. Therefore, a numerical experiment was set up to mathematically assess GS activity during the night (see **Figure 4B**). Nocturnal GS activity was intentionally reduced in steps of 10%, and 10 simulations of model states were conducted for each step. Simulations were accepted, when results for all states lay within the measured standard deviation. As can be seen in **Figure 4B**, the cumulative error of simulations was minimized for nocturnal GS activity between 20 and 50% of the *in vitro* activity. This agrees with the data of Choi et al. (1999), who showed that dithiothreitol increased the activity by about two-fold. Thus, we added a factor in the model by which GS can be down-regulated by the optimizer during the night.

## Photorespiration in the *hpr1-1* Mutant

As can be seen from the model structure in **Figure 3**, fluxes such as *HPR* summarize multiple enzymatic steps, for which kinetic parameters may deviate from those determined for individual enzymes that are rate-limiting under most conditions. Thus, for identification of the  $k_m$  of the *HPR* reaction a broad interval was set in order to integrate activity

of several enzymes and transporters, for which no parameter boundaries are known. This includes transport of Ser out of the mitochondria and into the peroxisomes, its de-amination by Ser-glyoxylate transaminase, the actual reduction by *HPR* and finally the phosphorylation of glycerate before its re-integration into the Calvin-Benson cycle. Most importantly, it is unclear whether in Col-0 *HPR* constitutes the rate-limiting step in the PR pathway.

Setting a broad interval for the *HPR* parameters created a problem for simulations in *hpr1-1*, because it allowed for a purely mathematical compensation of the low  $v_{max}$  in the mutant by choosing an adequately low  $k_m$ . To prevent this, the identified minimum of the  $k_m$  value for *HPR* in Col-0 was set as lower boundary for simulations of the *hpr1-1* mutant with the underlying assumption that the  $k_m$ , being a feature of a protein, cannot easily change. However, using this approach the simulated Ser pool was slightly higher than measured for the mutant at eCO<sub>2</sub> (**Figure 5**) albeit not at ambient. Opening of the lower boundary to allow a further 30% reduction of the  $k_m$  could correct this, as demonstrated by the simulations in **Figure 1B**, and was thus used as setting for all simulations.

## Observed Flux Dynamics

Using the parameter sets obtained from the simulations, flux rates at time points of harvest were calculated. **Figure 6** shows calculated flux rates for PR-relevant reactions. As expected, *HPR* flux was higher at ambient than eCO<sub>2</sub> ( $p < 2e-16$ ) due to the larger PR input. Similar, *GDC* and *SHMT* (**Figures 6A,B**) were increased at ambient CO<sub>2</sub> as compared to eCO<sub>2</sub> ( $p < 2e-16$ ). Surprisingly, *HPR* (**Figure 6C**) showed higher flux rates in the mutant as compared to wildtype ( $p < 2e-16$ ). This resulted from extremely high levels of Ser, which is the substrate in our compiled *HPR* reaction, and indicated a metabolic state clearly different from wildtype. For instance, the Ser levels already at the beginning of the day are substantially elevated in the mutant at ambient CO<sub>2</sub>. Moreover, in comparison to wildtype the *hpr1-1* mutant showed increased levels for *GDC* ( $p = 1.16e-10$ ). In contrast, the *SHMT* reaction tended to be increased in the wildtype, though this was not significant.

Flux within the GS/GOGAT cycle (**Figure 7**) was tightly linked to *PR*. For *GS* and *GOGAT* genotype and treatment effects were observed (treatment effect on *GS* and *GOGAT*:  $p < 2e-16$ ; genotype effect on *GS*:  $p < 2e-16$ ; genotype effect on *GOGAT*:  $p = 5.63e-14$ ). The highest flux was obtained at ambient CO<sub>2</sub> for *hpr1-1*, followed by Col-0 at ambient. For plants grown at eCO<sub>2</sub>, a slightly higher flux was observed for *hpr1-1* as compared to wildtype, supporting an earlier finding that PR takes place even at a CO<sub>2</sub> concentration of 1,000 ppm (Kraemer et al., 2021a). In summary, the mutant showed a higher turnover in the GS/GOGAT cycle compared to the wildtype, and this turnover was decreased at eCO<sub>2</sub>. However, flux of *NR* (**Figure 7C**) behaved differently. *NR* flux was higher in Col-0 and rose at eCO<sub>2</sub>, revealing significant genotype and treatment effects ( $p = 5.66e-11$  and  $p = 4.79e-07$ , respectively).

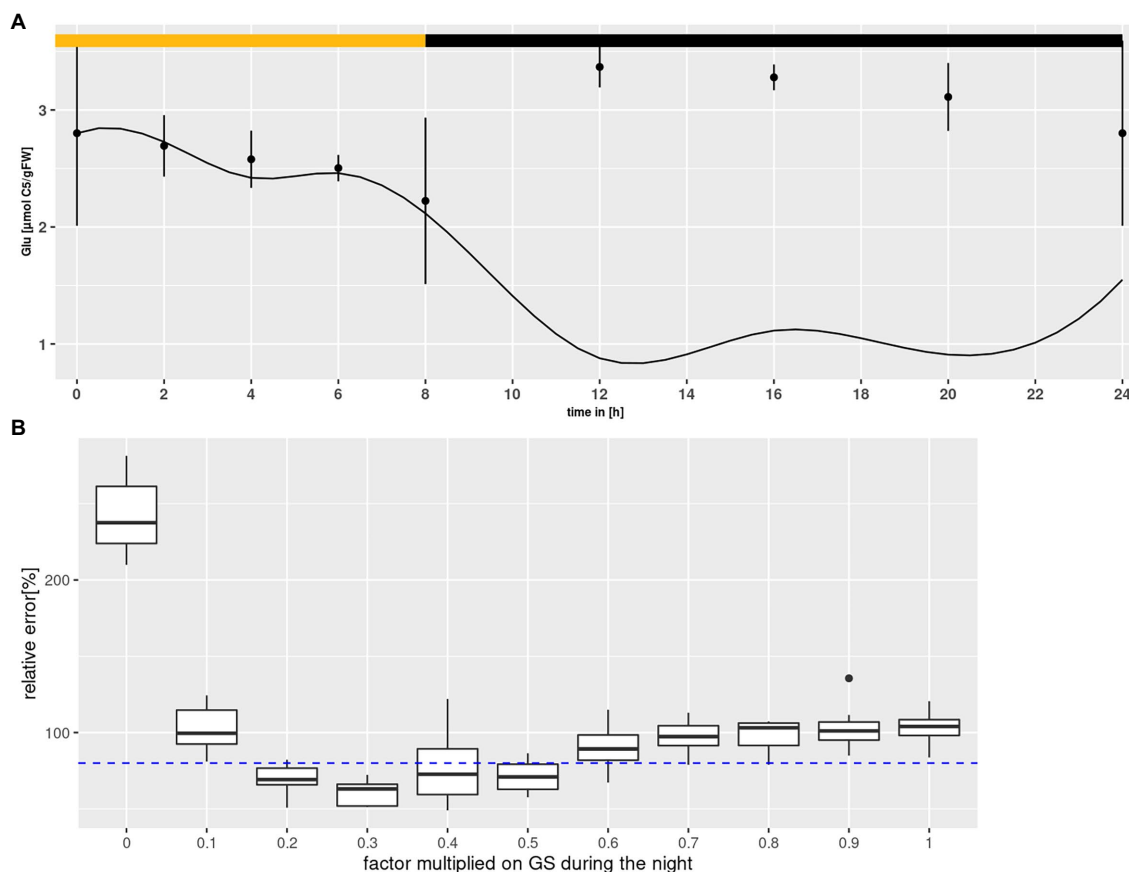


**FIGURE 4 |** Glutamine synthetase (GS) inactivation. **(A)** Diurnal course of glutamate for Col-0 at ambient CO<sub>2</sub> concentrations. Shown are mean with standard error ( $n=5$ ). Lines represent the mean of 10 simulations. Light phase indicated by yellow bar and dark phase indicated by black bar. **(B)** Error plotted against the factor multiplied with GS activity during the night. Each boxplot represents 10 simulations for Col-0 at ambient CO<sub>2</sub> concentrations. The dashed line indicates the threshold at which results for simulations of all states were accepted (see text for criteria).

## DISCUSSION

### Interaction of eCO<sub>2</sub> and N-Assimilation

Several studies have pointed out that eCO<sub>2</sub> decreases the N content of plant biomass (Bloom et al., 2014; Andrews et al., 2020). However, the underlying mechanism is unclear. Low stomatal conductance at high internal CO<sub>2</sub> concentrations could reduce nitrate availability, but in contrast to observations for wheat under eCO<sub>2</sub> (Del Pozo et al., 2007), we found no indications for reduced mineral content in *Arabidopsis* wildtype plants (**Supplementary Image 3A**). Although no consistent change of foliar nitrate was observed in the wildtype, it was significantly lower in the *hpr1-1* mutant especially under ambient CO<sub>2</sub>. This points to a restricted uptake capability in *hpr1-1*, probably because of energetic constraints (see below).

The alternative possibility that nitrate reduction was inhibited at eCO<sub>2</sub> (Bloom et al., 2014; Zhao et al., 2021) was also not supported in the current study. We found that the  $v_{\max}$  for NR increased at eCO<sub>2</sub> (**Figure 7C**), and the calculated NR flux was higher at eCO<sub>2</sub> in wildtype plants.

The observation that NR was consistently higher in Col-0 as compared to the *hpr1-1* mutant, which had high levels of free AA, further argues against insufficient N supply. Thus, our results are in support of reports favoring a dilution of total N to accompany increased carbon fixation and biomass formation under eCO<sub>2</sub> (Andrews et al., 2019). For eCO<sub>2</sub>, we found a higher ratio of NR to GDC (**Figure 8A**). Both fluxes feed into the pool of ammonium used for Gln synthesis. A low GDC contribution would reduce the load on the GS/GOGAT cycle, allowing a higher proportion of *de novo* N assimilation. Indeed, we calculated a lower flux for GS/GOGAT at eCO<sub>2</sub> (**Figures 7A,B**), demonstrating a tight link between PR and GS/GOGAT turnover. This link has also been shown by Häusler et al. (1994) and Wallsgrove et al. (1987), who reported that barley mutants lacking GS activity suffered under photorespiratory conditions. In addition, it is known that even short incubations at eCO<sub>2</sub> result in a reduction of GS and GOGAT activity (Guo et al., 2013; Wu et al., 2020). Our finding that the ratio of NR to GDC activity was elevated at eCO<sub>2</sub> in the wildtype as well as the mutant indicates that the GS/GOGAT cycle

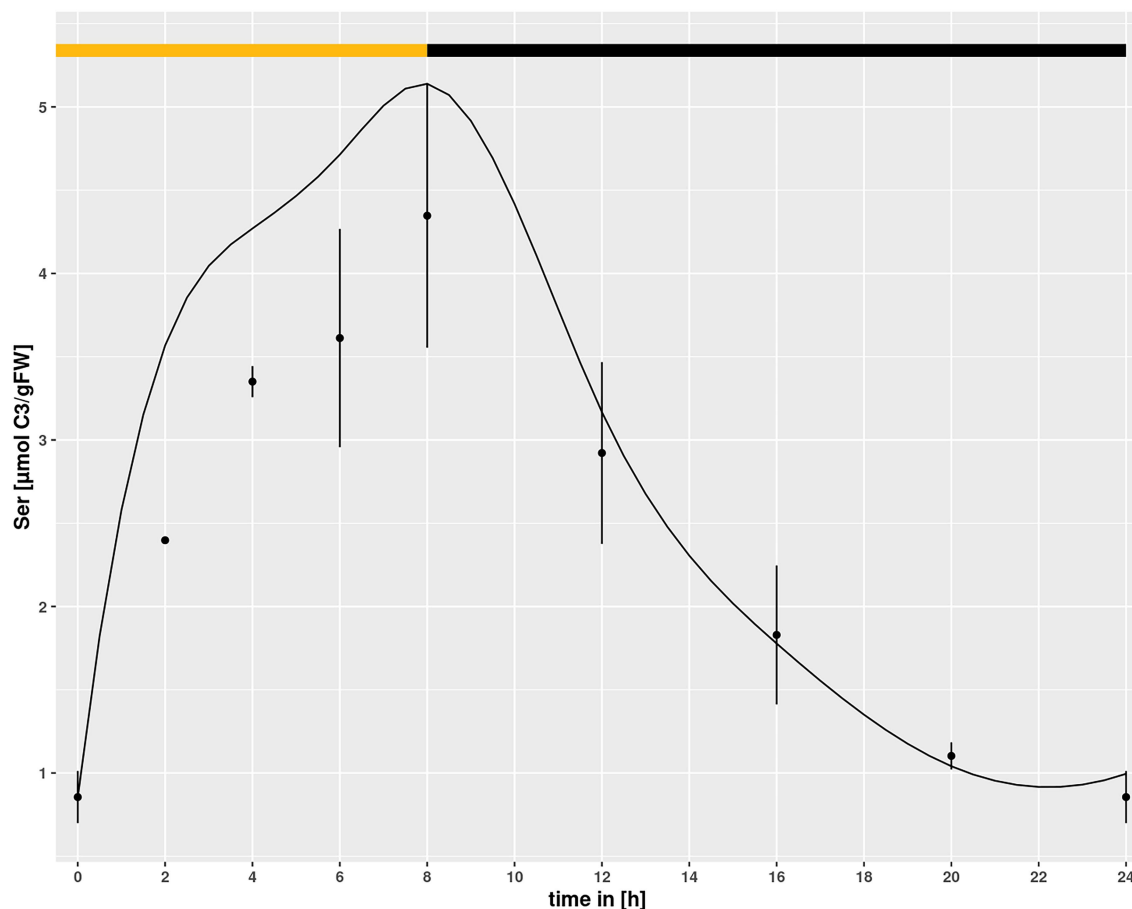


**FIGURE 5 |** Diurnal course of serine for *hpr1-1* at eCO<sub>2</sub> concentrations. Dots represent means with standard error ( $n=5$ ). Lines represent the mean of 20 simulations using the minimum of the km value of the simulations of Col-0 ambient CO<sub>2</sub> as lower boundary. The light phase is indicated by a yellow bar and dark phase indicated by black bar.

contained more newly assimilated N at eCO<sub>2</sub>, and this further argues against N starvation at eCO<sub>2</sub>.

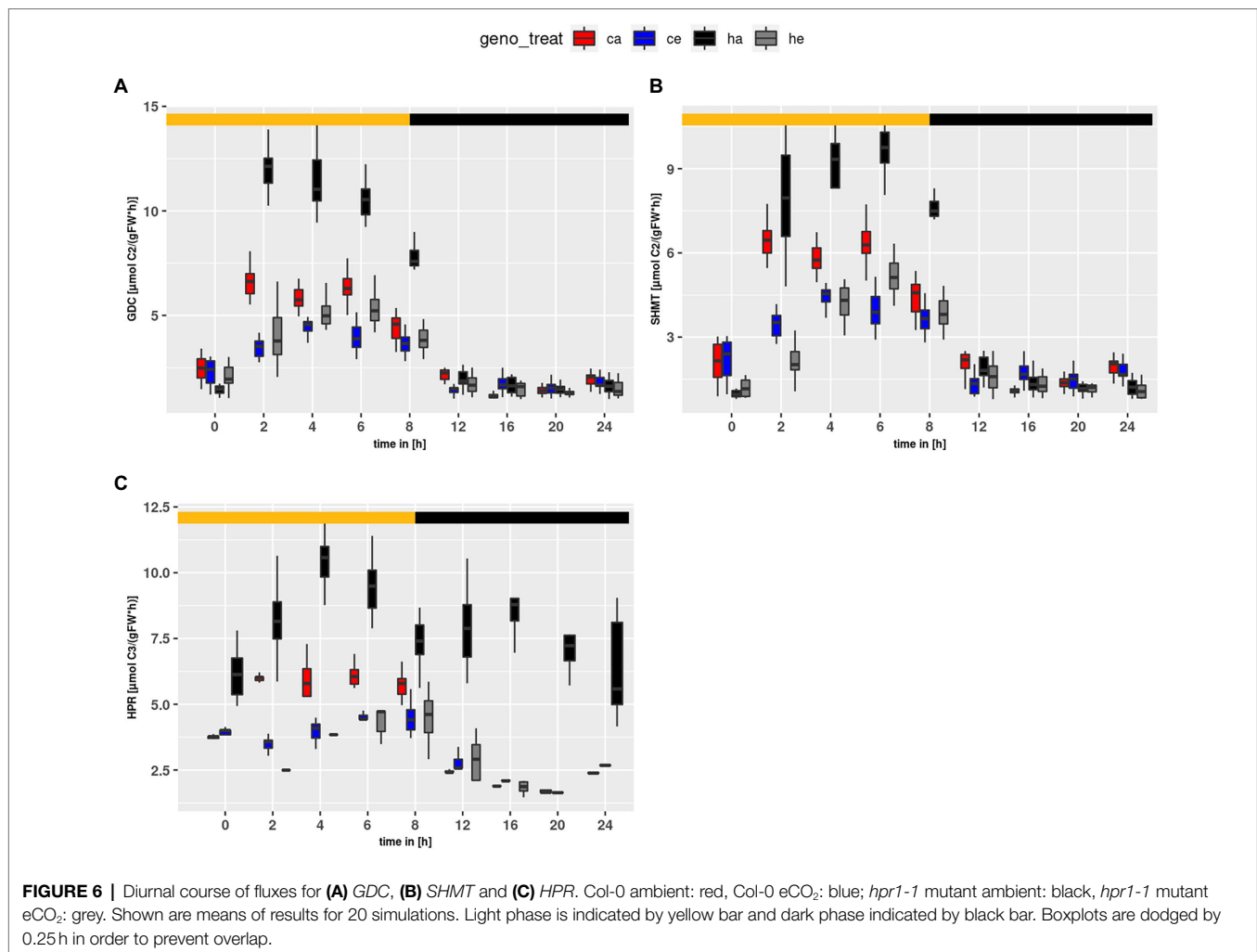
In a previous study comparing plants exposed to eCO<sub>2</sub> either short or long term, we revealed that PR allows deposition of already assimilated N in low carbon-containing AA like Gly and Ser, thus providing carbon skeletons for *de novo* N assimilation (Kraemer et al., 2021a). While this can explain photosynthetic acclimation to long-term eCO<sub>2</sub>, which results in reduced *PS* as well as *NR* rate, it does not explain an imbalance in the ratio of both fluxes. Whether sufficient N for the production of biomass was assimilated at eCO<sub>2</sub> should be reflected in the ratio of the carbon flux HP2BMEXP and the *de novo* N fixation by *NR*. **Figure 8B** shows a significant but not dramatic increase of this ratio at eCO<sub>2</sub>. Considering the increased *NR* flux, this indicates that carbon assimilation was even more stimulated than N fixation at eCO<sub>2</sub>, which would support the concept of N dilution at eCO<sub>2</sub> (Wong, 1990; Kuehny et al., 1991; Gifford et al., 2000; Taub and Wang, 2008). This is also substantiated by the strongly increased starch levels (**Supplementary Image 3B**). In the mutant, however, we and others (Timm et al., 2008) found a large pool of free

amino acids (**Figures 1, 2**), which apparently contradicts an increased C/N ratio.

### Phenotype of the *hpr1-1* Mutant

As mentioned above, an energetic constraint could be responsible for the metabolic disturbance in the mutant. As shown in **Figure 7**, the fluxes for *GS* and *GOGAT* are increased in *hpr1-1* as compared to wildtype especially at ambient CO<sub>2</sub>. Thus, large amounts of ATP and reduced ferredoxin are required to sustain synthesis of Glu, which is needed for the removal of glyoxylate. **Figure 8A** shows that the *NR*-to-*GDC* ratio was lowest for *hpr1-1* at ambient, thus indicating futile cycling of ammonium without net gain of biomass.

While a loss of cellular energy could explain the differences in biomass formation of wildtype and mutant at different CO<sub>2</sub> concentrations, which have already been described (Timm et al., 2008), futile cycling of already assimilated ammonium could be regarded as conflicting with high levels of amino acids in the mutant. Accumulation of starch, carboxylates and AA in the mutant could simply result from a slow growth rate as



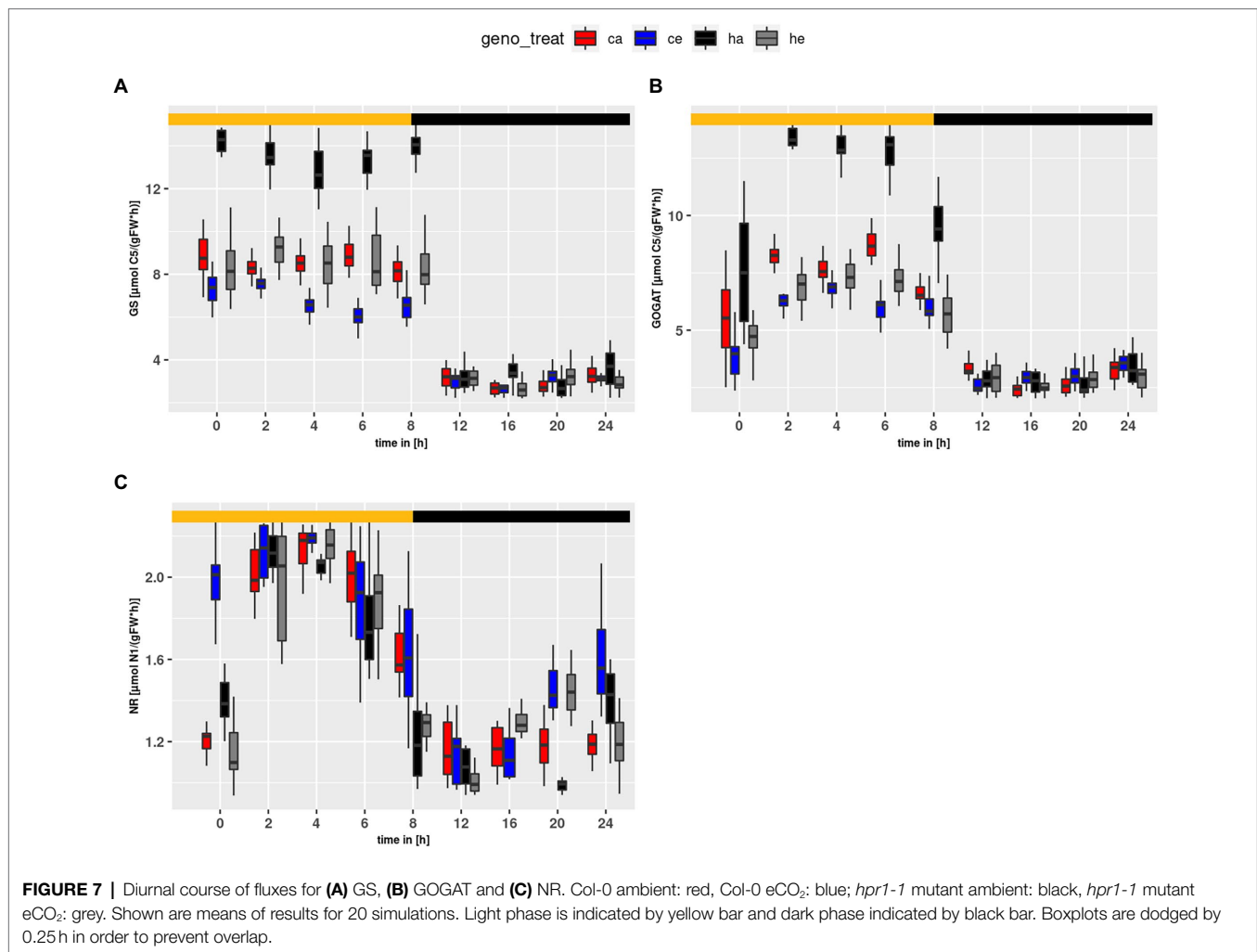
suggested by Génard et al. (2014), but than a reason different from resource limitation must underly stunted growth and chlorotic phenotype of *hpr1-1*.

A possible explanation could be poisoning by photorespiratory intermediates such as phosphoglycolate, glycolate or glyoxylate (Anderson, 1971; Dellero et al., 2016). As can be seen in **Figure 6** the GDC and SHMT fluxes are strongly increased in *hpr1-1* at ambient CO<sub>2</sub>. But still the HPR flux is substantially extended into the night. This shows that even after light-off photorespiratory intermediates had to be recycled, which were not metabolized during the day in spite of the increased GDC and SHMT activity. It can thus be assumed that phosphoglycolate accumulates during the day, and this would strongly inhibit triose-phosphate isomerase (Anderson, 1971), which would in turn block carbon assimilation in the Calvin-Benson cycle. But how should a bottleneck in the last step of the PR pathway cause accumulation of the early metabolites? As we have already described (Krämer et al., 2021a), simulations of a metabolic model for the *hpr1-1* mutant pointed to an additional source of glycolate, which is independent from oxygenation of ribulose-bisphosphate. A very likely candidate is the non-enzymatic oxidation of hydroxypyruvate by H<sub>2</sub>O<sub>2</sub> in the peroxisome, which

yields glycolate (Walton and Butt, 1981). This reaction is promoted by the large amount of Ser in the mutant at ambient CO<sub>2</sub>. Bao et al. (2021) showed that already a fourfold increase of Ser levels in the catalase mutant *cat2* caused a significant increase in hydroxypyruvate decarboxylation. Considering that Ser levels in *hpr1-1* were about tenfold higher than wildtype at the end of the day, it is highly likely that non-enzymatic decarboxylation of hydroxypyruvate takes place in *hpr1-1*. Thus, in the *hpr1-1* mutant more glycolate is produced in relation to photosynthetic carbon acquisition as compared to the wildtype. This would not only increase the probability of a toxic effect, but also cause additional loss of assimilated carbon in the form of CO<sub>2</sub>.

Besides toxication by photorespiratory intermediates, it would also be possible that an increased level of ammonium (**Figure 1C**) could interfere with ATP production, because it is in equilibrium with ammonia that acts as an uncoupling agent of ATP synthesis.

Finally, the metabolic bottleneck created by the *hpr1-1* mutation caused large amounts of C and N being bound in the form of Gly and Ser. As a consequence, the equilibrium of free amino-acids, brought about by transamination reactions, might be severely disturbed, and this could interfere with



protein synthesis in the shoot as well as the supply of the roots and other sinks with AA. Not only N but also C compounds show altered distributions in *hpr1-1* (Supplementary Image 1; Figure 2). Especially the carboxylates Cit, malate and fumarate, were significantly enriched, while glucose was reduced in *hpr1-1*. We did not detect a drop in foliar sucrose content, but the lowered nitrate content of *hpr1-1* shoots in ambient CO<sub>2</sub> might indicate low carbon supply to the root system. The low glucose level in leaves could result from enhanced use in the pentose-phosphate pathway as suggested by Li et al. (2019), who reported that high pentose-phosphate pathway activity could provide additional CO<sub>2</sub> that would alleviate the PR syndrome, but restrict biomass formation. A combination of the above described effects could contribute to the mutant phenotype of *hpr1-1*.

## CONCLUSION

We showed that the *hpr1-1* mutant suffers from several limitations. Besides a high demand for ATP and reducing equivalents for the increased turnover of the GS/GOGAT cycle, a possible

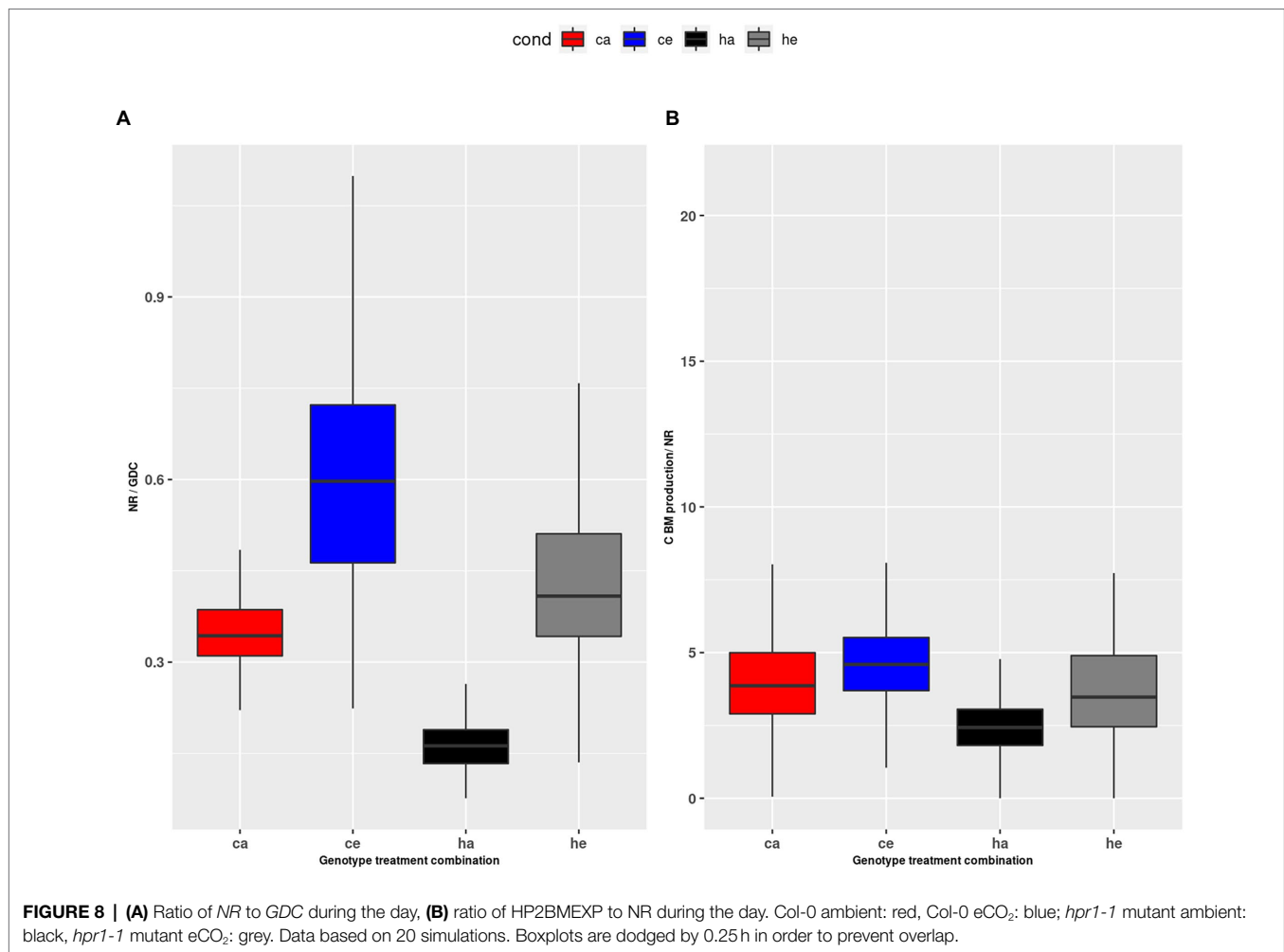
toxication by photorespiratory intermediates or NH<sub>4</sub><sup>+</sup> could interfere with biomass formation, and an unfavorable redistribution of N and C compounds could contribute to restricted biomass production. Our study confirms a tight link between PR and the GS/GOGAT cycle and adds to our understanding of how plant N assimilation is affected by eCO<sub>2</sub>.

## DATA AVAILABILITY STATEMENT

The raw data supporting the conclusions of this article can be found in the Supplementary Material, further inquiries can be directed to the corresponding author.

## AUTHOR CONTRIBUTIONS

KK and AH designed the study and wrote the manuscript. KK developed the model. KK and JB conducted the experiments. All authors contributed to the article and approved the submitted version.



## FUNDING

KK was supported by a scholarship “Landesgraduiertenförderung (LGF)” of the Federal State of Baden-Wuerttemberg (Germany).

## ACKNOWLEDGMENTS

The authors would like to thank Hermann Bauwe and Stefan Timm for a generous gift of seeds of the *hpr1-1*

mutant used in this study. Nadja Beuttenmüller and Annika Allinger are acknowledged for expert plant cultivation.

## SUPPLEMENTARY MATERIAL

The Supplementary Material for this article can be found online at: <https://www.frontiersin.org/articles/10.3389/fpls.2022.897924/full#supplementary-material>

## REFERENCES

- Anderson, L. (1971). Chloroplast and cytoplasmic enzymes II. Pea leaf triose phosphate isomerases. *Biochim. Biophys. Acta* 22, 237–244.
- Andrews, M., Condrón, L. M., Kemp, P. D., Topping, J. F., Lindsey, K., Hodge, S., et al. (2019). Elevated CO<sub>2</sub> effects on nitrogen assimilation and growth of C<sub>3</sub> vascular plants are similar regardless of N-form assimilated. *J. Exp. Bot.* 70, 683–690. doi: 10.1093/jxb/ery371
- Andrews, M., Condrón, L. M., Kemp, P. D., Topping, J. F., Lindsey, K., Hodge, S., et al. (2020). Will rising atmospheric CO<sub>2</sub> concentration inhibit nitrate assimilation in shoots but enhance it in roots of C<sub>3</sub> plants? *Physiol. Plantarum* 170, 40–45. doi: 10.1111/ppl.13096
- Atkinson, N., Leitão, N., Orr, D. J., Meyer, M. T., Carmo-Silva, E., Griffiths, H., et al. (2017). Rubisco small subunits from the unicellular green alga *Chlamydomonas* complement Rubisco-deficient mutants of *Arabidopsis*. *New Phytol.* 214, 655–667. doi: 10.1111/nph.14414
- Bao, H., Morency, M., Rianti, W., Saeheng, S., Roje, S., Weber, A. P. M., et al. (2021). Catalase protects against nonenzymatic decarboxylations during photorespiration in *Arabidopsis thaliana*. *Plant Direct* 5:e366. doi: 10.1002/pld3.366
- Bauwe, H. (2017). “Measurement of enzyme activities,” in *Photorespiration: Methods and Protocols*. eds. A. R. Fernie, H. Bauwe and A. P. Weber (New York, NY: Springer New York), 31–50.
- Berardini, T. Z., Reiser, L., Li, D., Mezheritsky, Y., Muller, R., Strait, E., et al. (2015). The arabidopsis information resource: making and mining the “gold

- standard” annotated reference plant genome. *Genesis* 53, 474–485. doi: 10.1002/dvg.22877
- Berteli, F., Corrales, E., Guerrero, C., Ariza, M. J., Pliego, F., and Valpuesta, V. (1995). Salt stress increases ferredoxin-dependent glutamate synthase activity and protein level in the leaves of tomato. *Physiol Plantarum* 93, 259–264. doi: 10.1111/j.1399-3054.1995.tb02226.x
- Bloom, A. J. (2015). Photorespiration and nitrate assimilation: a major intersection between plant carbon and nitrogen. *Photosynth. Res.* 123, 117–128. doi: 10.1007/s11120-014-0056-y
- Bloom, A. J., Burger, M., Kimball, B. A., and Pinter, P. J. (2014). Nitrate assimilation is inhibited by elevated CO<sub>2</sub> in field-grown wheat. *Nat. Clim. Chang.* 4, 477–480. doi: 10.1038/nclimate2183
- Brauner, K., Hörmiller, I., Nägele, T., and Heyer, A. G. (2014). Exaggerated root respiration accounts for growth retardation in a starchless mutant of *Arabidopsis thaliana*. *Plant J.* 79, 82–91. doi: 10.1111/tj.12555
- Cheung, C. M., Poolman, M. G., Fell, D. A., Ratcliffe, R. G., and Sweetlove, L. J. (2014). A diel flux balance model captures interactions between light and dark metabolism during day-night cycles in C<sub>3</sub> and crassulacean acid metabolism leaves. *Plant Physiol.* 165, 917–929. doi: 10.1104/pp.113.234468
- Choi, Y. A., Kim, S. G., and Kwon, Y. M. (1999). The plastidic glutamine synthetase activity is directly modulated by means of redox change at two unique cysteine residues. *Plant Sci.* 149, 175–182. doi: 10.1016/S0168-9452(99)00163-6
- Cousins, A. B., and Bloom, A. J. (2004). Oxygen consumption during leaf nitrate assimilation in a C<sub>3</sub> and C<sub>4</sub> plant: The role of mitochondrial respiration. *Plant Cell Environ.* 27, 1537–1545. doi: 10.1111/j.1365-3040.2004.01257.x
- Del Pozo, A., Pérez, P., Gutiérrez, D., Alonso, A., Morcuende, R., and Martínez-Carrasco, R. (2007). Gas exchange acclimation to elevated CO<sub>2</sub> in upper-sunlit and lower-shaded canopy leaves in relation to nitrogen acquisition and partitioning in wheat grown in field chambers. *Environ. Exp. Bot.* 59, 371–380. doi: 10.1016/j.envexpbot.2006.04.009
- Dellero, Y., Jossier, M., Schmitz, J., Maurino, V. G., and Hodges, M. (2016). Photorespiratory glycolate – glyoxylate metabolism. *J. Exp. Bot.* 67, 3041–3052. doi: 10.1093/jxb/erw090
- Dietz, K. J., and Hell, R. (2015). Thiol switches in redox regulation of chloroplasts: balancing redox state, metabolism and oxidative stress. *Biol. Chem.* 396, 483–494. doi: 10.1515/hsz-2014-0281
- Gauthier, P. P. G., Bligny, R., Gout, E., Mahé, A., Nogués, S., Hodges, M., et al. (2010). *In folio* isotopic tracing demonstrates that nitrogen assimilation into glutamate is mostly independent from current CO<sub>2</sub> assimilation in illuminated leaves of *Brassica napus*. *New Phytol.* 185, 988–999. doi: 10.1111/j.1469-8137.2009.03130.x
- Génard, M., Baldazzi, V., and Gibon, Y. (2014). Metabolic studies in plant organs: don't forget dilution by growth. *Front. Plant Sci.* 5:85. doi: 10.3389/fpls.2014.00085
- Gifford, R. M., Barrett, D. J., and Lutze, J. L. (2000). The effects of elevated CO<sub>2</sub> on the C:N and C:P mass ratios of plant tissues. *Plant Soil* 224, 1–14. doi: 10.1023/A:1004790612630
- Graham, L., and Aprison, M. (1966). Fluorometric determination of aspartate, glutamate, and gamma-Aminobutyrate in nerve tissue using Enzymic methods. *Anal. Biochem.* 15, 487–497. doi: 10.1016/0003-2697(66)90110-2
- Guan, X. Q., Zhao, S. J., Li, D. Q., and Shu, H. R. (2004). Photoprotective function of photorespiration in several grapevine cultivars under drought stress. *Photosynthetica* 42, 31–36. doi: 10.1023/B:PHOT.0000040566.55149.52
- Guo, H., Sun, Y., Li, Y., Liu, X., Ren, Q., Zhu-Salzman, K., et al. (2013). Elevated CO<sub>2</sub> modifies N acquisition of *Medicago truncatula* enhancing N fixation and reducing nitrate uptake from soil. *PLoS One* 8:e81373. doi: 10.1371/journal.pone.0081373
- Häusler, R. E., Lea, P. J., and Leegood, R. C. (1994). Control of photosynthesis in barley leaves with reduced activities of glutamine synthetase or glutamate synthase - II. Control of electron transport and CO<sub>2</sub> assimilation. *Planta* 194, 418–435. doi: 10.1007/BF00197543
- Hodges, M. (2002). Enzyme redundancy and the importance of 2-oxoglutarate in plant ammonium assimilation. *J. Exp. Bot.* 53, 905–916. doi: 10.1093/jxb/53.370.905
- Huma, B., Kundu, S., Poolman, M. G., Kruger, N. J., and Fell, D. A. (2018). Stoichiometric analysis of the energetics and metabolic impact of photorespiration in C<sub>3</sub> plants. *Plant J.* 96, 1228–1241. doi: 10.1111/tj.14105
- IPCC (2014). “Summary for Policymakers.” in *Climate Change 2014: Mitigation of climate change. Contribution of Working Group III to the Fifth Assessment Report of the Intergovernmental Panel on Climate Change*; April 2014.
- Jauregui, I., Aparicio-Tejo, P. M., Avila, C., Cañas, R., Sakalauskiene, S., and Aranjuelo, I. (2016). Root-shoot interactions explain the reduction of leaf mineral content in *Arabidopsis* plants grown under elevated [CO<sub>2</sub>] conditions. *Physiol. Plant.* 158, 65–79. doi: 10.1111/pp.12417
- Koffler, B. E., Bloem, E., Zellnig, G., and Zechmann, B. (2013). High resolution imaging of subcellular glutathione concentrations by quantitative immunoelectron microscopy in different leaf areas of *Arabidopsis*. *Micron* 45, 119–128. doi: 10.1016/j.micron.2012.11.006
- Kraemer, K., Kepp, G., Brock, J., Stutz, S., and Heyer, A. G. (2021a). Acclimation to elevated CO<sub>2</sub> affects the C/N balance by reducing de novo N-assimilation. *Physiol Plantarum* 174:e13615. doi: 10.1111/pp.13615
- Kraemer, K., Kraemer, J., and Heyer, A. G. (2021b). Paropt: parameter optimizing of ODE-Systems. Available at: <https://cran.r-project.org/package=paropt> (Accessed June 13, 2022).
- Kuehny, J. S., Peet, M. M., Nelson, P. V., and Willits, D. H. (1991). Nutrient dilution by starch in CO<sub>2</sub>-enriched chrysanthemum. *J. Exp. Bot.* 42, 711–716. doi: 10.1093/jxb/42.6.711
- Küstner, L., Nägele, T., and Heyer, A. G. (2019). Mathematical modeling of diurnal patterns of carbon allocation to shoot and root in *Arabidopsis thaliana*. *Npj Syst. Biol. Appl.* 5, 1–11. doi: 10.1038/s41540-018-0080-1
- Li, J., Weraduwage, S. M., Preiser, A. L., Tietz, S., Weise, S. E., Strand, D. D., et al. (2019). A cytosolic bypass and G6P shunt in plants lacking Peroxisomal Hydroxypyruvate Reductase. *Plant Physiol.* 180, 783–792. doi: 10.1104/pp.19.00256
- Nunes-Nesi, A., Fernie, A. R., and Stitt, M. (2010). Metabolic and signaling aspects underpinning the regulation of plant carbon nitrogen interactions. *Mol. Plant* 3, 973–996. doi: 10.1093/mp/ssp049
- Pérez-de la Mora, M., Méndez-Franco, J., Salceda, R., and Riesgo-Escovar, J. R. (1989). A glutamate dehydrogenase-based method for the assay of L-glutamic acid: formation of pyridine nucleotide fluorescent derivatives. *Anal. Biochem.* 180, 248–252. doi: 10.1016/0003-2697(89)90425-9
- Rebeille, F., Neuburger, M., and Douce, R. (1994). Interaction between glycine decarboxylase, serine hydroxymethyltransferase and tetrahydrofolate polyglutamates in pea leaf mitochondria. *Biochem. J.* 302, 223–228. doi: 10.1042/bj3020223
- Scholl, R. L., Harper, J. E., and Hageman, R. H. (1974). Improvements of the nitrite color development in assays of nitrate Reductase by Phenazine Methosulfate and zinc acetate 1. *Plant Physiol.* 53, 825–828. doi: 10.1104/pp.53.6.825
- Selinski, J., and Scheibe, R. (2019). Malate valves: old shuttles with new perspectives. *Plant Biol.* 21, 21–30. doi: 10.1111/plb.12869
- Sharkey, T. D. (1988). Estimating the rate of photorespiration in leaves. *Physiol Plantarum* 73, 147–152. doi: 10.1111/j.1399-3054.1988.tb09205.x
- Shih, P. M., Occhialini, A., Cameron, J. C., Andralojc, P. J., Parry, M. A., and Kerfeld, C. A. (2015). Biochemical characterization of predicted Precambrian RuBisCO. *Nat. Commun.* 7, 1–11. doi: 10.1038/ncomms10382
- Silveira, J. A. G., Viégas, R., da Rocha, I. M. A., Moreira, A. C. D. O. M., Moreira, R. D. A., and Oliveira, J. T. A. (2003). Proline accumulation and glutamine synthetase activity are increased by salt-induced proteolysis in cashew leaves. *J. Plant Physiol.* 160, 115–123. doi: 10.1078/0176-1617-00890
- Stitt, M., and Zeeman, S. C. (2012). Starch turnover: pathways, regulation and role in growth. *Curr. Opin. Plant Biol.* 15, 282–292. doi: 10.1016/j.cpb.2012.03.016
- Szulejko, J. E., Kumar, P., Deep, A., and Kim, K. H. (2017). Global warming projections to 2100 using simple CO<sub>2</sub> greenhouse gas modeling and comments on CO<sub>2</sub> climate sensitivity factor. *Atmos. Pollut. Res.* 8, 136–140. doi: 10.1016/j.apr.2016.08.002
- Taub, D. R., and Wang, X. (2008). Why are nitrogen concentrations in plant tissues lower under elevated CO<sub>2</sub>? A critical examination of the hypotheses. *J. Integr. Plant Biol.* 50, 1365–1374. doi: 10.1111/j.1744-7909.2008.00754.x
- Tcherkez, G., Mahe, A., Gauthier, P., Mauve, C., Gout, E., Bligny, R., et al. (2009). *In folio* respiratory fluxomics revealed by <sup>13</sup>C isotopic labeling and H/D isotope effects highlight the noncyclic nature of the tricarboxylic acid “cycle” in illuminated leaves. *Plant Physiol.* 151, 620–630. doi: 10.1104/pp.109.142976
- Timm, S., Nunes-Nesi, A., Florian, A., Eisenhut, M., Morgenthal, K., Wirtz, M., et al. (2021). Metabolite profiling in *arabidopsis thaliana* with moderately

- impaired photorespiration reveals novel metabolic links and compensatory mechanisms of photorespiration. *Meta* 11:391. doi: 10.3390/metabo11060391
- Timm, S., Nunes-Nesi, A., Morgenthal, K., Wienkoop, S., Keerberg, O., Pärnik, T., et al. (2008). A cytosolic pathway for the conversion of Hydroxypyruvate to Glycerate during photorespiration in Arabidopsis. *Plant Cell* 20, 2848–2859. doi: 10.1105/tpc.108.062265
- Vega-Mas, I., Asier, S., and Marino, D. (2015). High-throughput quantification of ammonium content in Arabidopsis. *Bio-protocol* 5, 14–17. doi: 10.21769/BioProtoc.1559
- Voss, I., Sunil, B., Scheibe, R., and Raghavendra, A. S. (2013). Emerging concept for the role of photorespiration as an important part of abiotic stress response. *Plant Biol.* 15, 713–722. doi: 10.1111/j.1438-8677.2012.00710.x
- Wallsgrave, R. M., Turner, J. C., Hall, N. P., Kendall, A. C., and Bright, S. W. J. (1987). Barley mutants lacking chloroplast glutamine Synthetase—biochemical and genetic analysis. *Plant Physiol.* 83, 155–158. doi: 10.1104/pp.83.1.155
- Walton, N. J., and Butt, V. S. (1981). Metabolism and decarboxylation of glycollate and serine in leaf peroxisomes. *Planta* 153, 225–231. doi: 10.1007/BF00383891
- Wong, S. C. (1990). Elevated atmospheric partial pressure of CO<sub>2</sub> and plant growth - II. Non-structural carbohydrate content in cotton plants and its effect on growth parameters. *Photosynth. Res.* 23, 171–180. doi: 10.1007/BF00035008
- Wu, F., Sun, X., Hu, X., Zou, B., Lin, N., Lin, J., et al. (2020). Response of nitrogen metabolism in masson pine needles to elevated CO<sub>2</sub>. *Forests* 11, 1–13. doi: 10.3390/F11040390
- Xu, G., Fan, X., and Miller, A. J. (2012). Plant nitrogen assimilation and use efficiency. *Annu. Rev. Plant Biol.* 63, 153–182. doi: 10.1146/annurev-arplant-042811-105532
- Zhao, H.-L., Chang, T.-G., Xiao, Y., and Zhu, X.-G. (2021). Potential metabolic mechanisms for inhibited chloroplast nitrogen assimilation under high CO<sub>2</sub>. *Plant Physiol.* 187, 1812–1833. doi: 10.1093/plphys/kiab345

**Conflict of Interest:** The authors declare that the research was conducted in the absence of any commercial or financial relationships that could be construed as a potential conflict of interest.

**Publisher's Note:** All claims expressed in this article are solely those of the authors and do not necessarily represent those of their affiliated organizations, or those of the publisher, the editors and the reviewers. Any product that may be evaluated in this article, or claim that may be made by its manufacturer, is not guaranteed or endorsed by the publisher.

Copyright © 2022 Krämer, Brock and Heyer. This is an open-access article distributed under the terms of the Creative Commons Attribution License (CC BY). The use, distribution or reproduction in other forums is permitted, provided the original author(s) and the copyright owner(s) are credited and that the original publication in this journal is cited, in accordance with accepted academic practice. No use, distribution or reproduction is permitted which does not comply with these terms.